STEREO/SECCHI/EUVI Calibration and Measurement Algorithms Document (CMAD)

Version 1.0 / 30 June 2021 – Initial release

Version 1.1 / 06 December 2021 – Updated references

1. Introduction

The Extreme Ultraviolet Imager (EUVI) is an EUV telescope that belongs to the Sun Earth Connection Coronal and Heliospheric Investigation (SECCHI) instrument suite aboard the twin Solar Terrestrial Relations Observatory (STEREO) spacecraft. It covers the innermost region observed by SECCHI, from the solar surface up to the heliocentric distance of 1.7 R$_\odot$. The EUVI was built on its predecessor, EIT (Extreme-ultraviolet Imaging Telescope, Delaboudinière et al., et al. 1995) aboard the Solar and Heliospheric Observatory (SOHO), with several performance improvements including better spatial resolution and a higher image cadence. It observes the chromosphere to the low corona in the same four wavelength channels (17.1, 19.5, 28.4, and 30.4 nm) as EIT. These channels contain spectral lines Fe IX (~0.7 MK), Fe XII (~1.5 MK), Fe XV (~2.0 MK), and He II (~0.01 MK), respectively. A complete description of the EUVI is given in Wuelser et al. (2004) and Howard et al. (2008). The designs of the EUVI-A and EUVI-B on STEREO-A and STEREO-B were identical.

The main goal of the EUVI is to observe coronal mass ejections (CMEs) as they take place in the low corona. The EUVI plays an essential role in addressing the SECCHI science objectives such as,

- How do flux systems interact during the CME initiation, and what is the role of magnetic reconnection?
- What is the 3-dimensional structure of CMEs at their formation?
- What is the 3-dimensional structure of active regions, coronal loops, helmet streamers, etc.?
- What are the low coronal responses to CMEs?

As demonstrated by EIT/SOHO, EUV imagers in EUVI's wavelength channels are very useful for detecting signatures of CMEs observed by coronagraphs.

Figure 1 shows the mechanical design of the EUVI telescope. EUV radiation first experiences the entrance filter that blocks most of the UV, visible and IR radiation, and then passes through an aperture selector to one of the four quadrants of the optics. Each quadrant of the primary and secondary mirror is coated with a narrow-band, multilayer tuned to one of the four lines. After reflection by the secondary mirror, the radiation goes through a filter wheel for further suppression of the UV to IR radiation (stay light).

The filter wheel close to the focal plane has four slots, two hosting redundant 150 nm thick aluminum filter (also used for the entrance filter). The third slot is occupied by a doubly thick aluminum filter, and the fourth slot is open. The positions are called, S1, S2, DBL and OPEN, respectively. Most images in normal operations have been taken with S1.

Figure 1. EUVI cross section
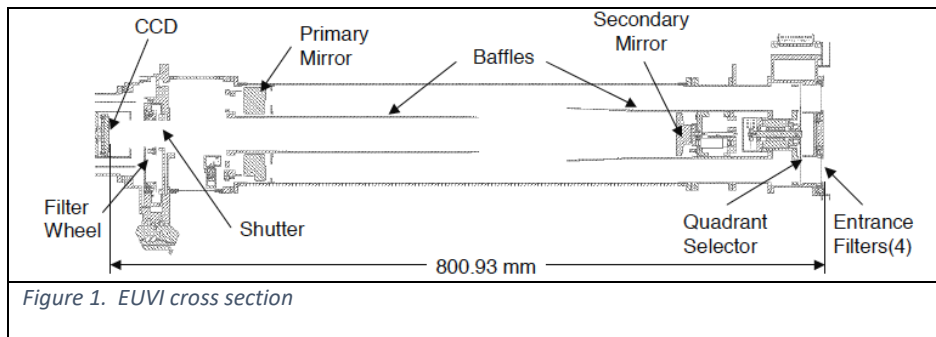
In synoptic observations, images in 17.1 nm channel were taken in the highest cadence until May 2009 for the stereoscopy of coronal loops, which appear sharper than in other channels. However, as the twin STEREO drifted further from each other and the stereoscopy of coronal loops became increasingly more difficult, the 19.5 nm channel became the channel of the highest cadence. This channel may be better suited to observe the low coronal signatures of CMEs, such as coronal dimmings and EUV waves.

The various algorithms described in this document are listed below

Section 2	Conversion from Level 0.5 to Level 1
Section 3	EUVI Temperature Response
Section 4	EUVI Wavelet

1.1   Purpose

This document describes the process used to convert from raw EUVI Level 0 images to calibrated Level 1 images, and the subsequent derivation of the temperature response. The Level 0 data are stored in FITS format, as described in [PIPELINE]. All calibration files needed to compute the temperature response are distributed as part of the SECCHI software package in SolarSoft.

1.2   Contents

Section 2 describes the procedure used to convert EUVI images from raw Level 0 to calibrated Level 1. In order to derive physical parameters such as temperature and density (Level 2), it is necessary to know how the expected flux depends on the temperature.   Section A.3 describes how the temperature response is calculated.

References

[PIPELINE] STEREO/SECCHI Level-0 to Level-0.5 FITS Pipeline CMAD, STEREO_SECCHI_Reduce_CMAD_20211206.pdf, Version 1.1, 06 December 2021

Delaboudinière, J.-P., Artzner, G.E., Brunaud, J., Gabriel, A.H., Hochedez, J.F., Millier, F., Song, X.Y., Au, B., Dere, K.P., Howard, R.A., Kreplin, R., Michels, D.J., Moses, J.D., Defise, J.M., Jamar, C., Rochus, P., Chauvineau, J.P., Marioge, J.P., Catura, R.C., Lemen, J.R., Shing, L., Stern, R.A., Gurman, J.B., Neupert, W.M., Maucherat, A., Clette, F., Cugnon, P., van Dessel, E.L.: 1995, EIT: Extreme-Ultraviolet Imaging Telescope for the SOHO Mission. Solar Phys. 162, 291.

Howard, R. A., Moses, J. D., Vourlidas, A., Newmark, J. S., Socker, D. G., Plunkett, S. P.; Korendyke, C. M., Cook, J. W., Hurley, A., Davila, J. M., Thompson, W. T., St Cyr, O. C.; Mentzell, E., Mehalick, K., Lemen, J. R., Wuelser, J. P., Duncan, D. W., Tarbell, T. D.; Wolfson, C. J., Moore, A. Harrison, R. A., Waltham, N. R., Lang, J., Davis, C. J.; Eyles, C. J., Mapson-Menard, H., Simnett, G. M., Halain, J. P., Defise, J. M., Mazy, E.; Rochus, P., Mercier, R., Ravet, M. F., Delmotte, F., Auchere, F., Delaboudiniere, J. P.; Bothmer, V., Deutsch, W., Wang, D., Rich, N., Cooper, S., Stephens, V., Maahs, G.; Baugh, R., McMullin, D., Carter, T., 2008, Sun Earth Connection Coronal and Heliospheric Investigation (SECCHI), *Space Sci. Rev.*, **136**, 67–115.

Wuelser, J.-P., Lemen, J.R., Tarbell, T.D., Wolfson, C.J., Cannon, J.C., Carpenter, B.A., Duncan, D.W., Gradwohl, G.S., Meyer, S.B., Moore, A.S., Navarro, R.L., Pearson, J.D., Rossi, G.R., Springer, L.A., Howard, R.A., Moses, J.D., Newmark, J.S., Delaboudiniere, J.- P., Artzner, G.E., Auchere, F., Bougnet, M., Bouyries, P., Bridou, F., Clotaire, J.-Y., Colas, G., Delmotte, F., Jerome, A., Lamare, M., Mercier, R., Mullot, M., Ravet, M.-F., Song, X., Bothmer, V., Deutsch, W.: 2004, EUVI: the STEREO-SECCHI extreme ultraviolet imager. In: Fineschi, S., Gummin, M.A. (eds.) Telescopes and Instrumentation for So- lar Astrophysics, Society of Photo-Optical Instrumentation Engineers (SPIE) Conference Series 5171, 111.

2. Conversion from Level 0.5 to Level 1

2.1 Overview

Conversion of SECCHI telemetry into Level 0.5 FITS files is described in **[PIPELINE]**. Here we describe the process of converting from raw Level 0.5 data to calibrated Level 1 data. This procedure is applied through the IDL routine `secchi_prep.pro` in the SolarSoft library. **[SECCHI_PREP]** gives an overview of the SECCHI_PREP routine.

2.1.1 Heritage

EUVI follows the calibration and reduction processes established in previous solar missions involving EUV telescopes, such as SOHO/EIT and TRACE. The analysis software follows the approach established by the Yohkoh mission in the 1990s, to process level0 data to higher-level data using *prep routines in SolarSoft.

2.1.2 Product Description

The process of applying calibration to EUVI Level 0.5 data to produce Level 1 data consists of converting raw detector signals in data numbers (DN) into the number of photons per sec (ph/s) units. Under the default settings, the level 1 images produced by secchi_prep represent the number of photons *incident* on the CCD detector. We discuss specific corrections later in this section. Unless otherwise specified, the output image is the same size and format as the input image, with each input and output pixel in a one-to-one correspondence with each other

2.2   Theoretical Description

EUVI follows the same photometric calibration procedures as other EUV telescopes. Following Dere at al. 2000, for example, the recorded signal on the detectors, S (in DN s^{-1} pix^{-1}) relates to the incoming solar spectral flux, F (cm^{-2} s^{-1} sr^{-1} Å^{-1}) as

$$S = \frac{A\alpha_{pix}}{G} \int \frac{T_{Filt}R_M}{f^2} QE \frac{hc}{\varphi\lambda} F(\lambda)d\lambda \tag{1}$$

Where A is the aperture (in cm^2), α_{pix} is the pixel area (in cm^2), G is the gain (15 e/DN), T_{filt} is the combined transmission of the entrance and analysis filter, R_M is the combined reflectivity of the primary and secondary mirror, f is the focal length (in cm) , QE is the quantum efficiency of the CCD at wavelength λ (in Å), h the Plank constant, c the light speed, and φ the work function of silicon (3.65 eV/ph). All variables are functions of wavelength except for A, α_{pix}, G and f.

It is customary to characterize the throughput of EUV telescopes in terms of the effective area A_{eff}

$$A_{eff} = A\, T_{Filt}R_M QE \tag{2}$$

Another useful quantity is the conversion factor of photons/DN, P_D,

$$P_D = \frac{G\varphi\lambda}{hc} = 15 \times 3.65 \times \frac{\lambda}{12389.6} = 4.4 \times 10^{-3}\lambda \tag{3}$$

Because EUVI uses broadband filters, the recorded signals on the images represent integrated solar flux over the given passband. The component calibrations are also performed largely at a single wavelength so only a single value is used for T_{filt}, R_M and QE in the reduction procedure. In addition we define the Level 1 images in units of ph/s rather than spectral flux, which simplfies the Level 1 calibration.

EUVI_PREP calibrates the input level 0.5 images *I* (in DN) to the level 1 images *O* (in ph/s) by calling EUVI_CORRECTION. The procedure subtracts the CCD bias, divides by the exposure time, t_{exp} , normalizes to the OPEN filter wheel position, N (*for calibration purposes only*), and converts DN to photons/second. Namely,
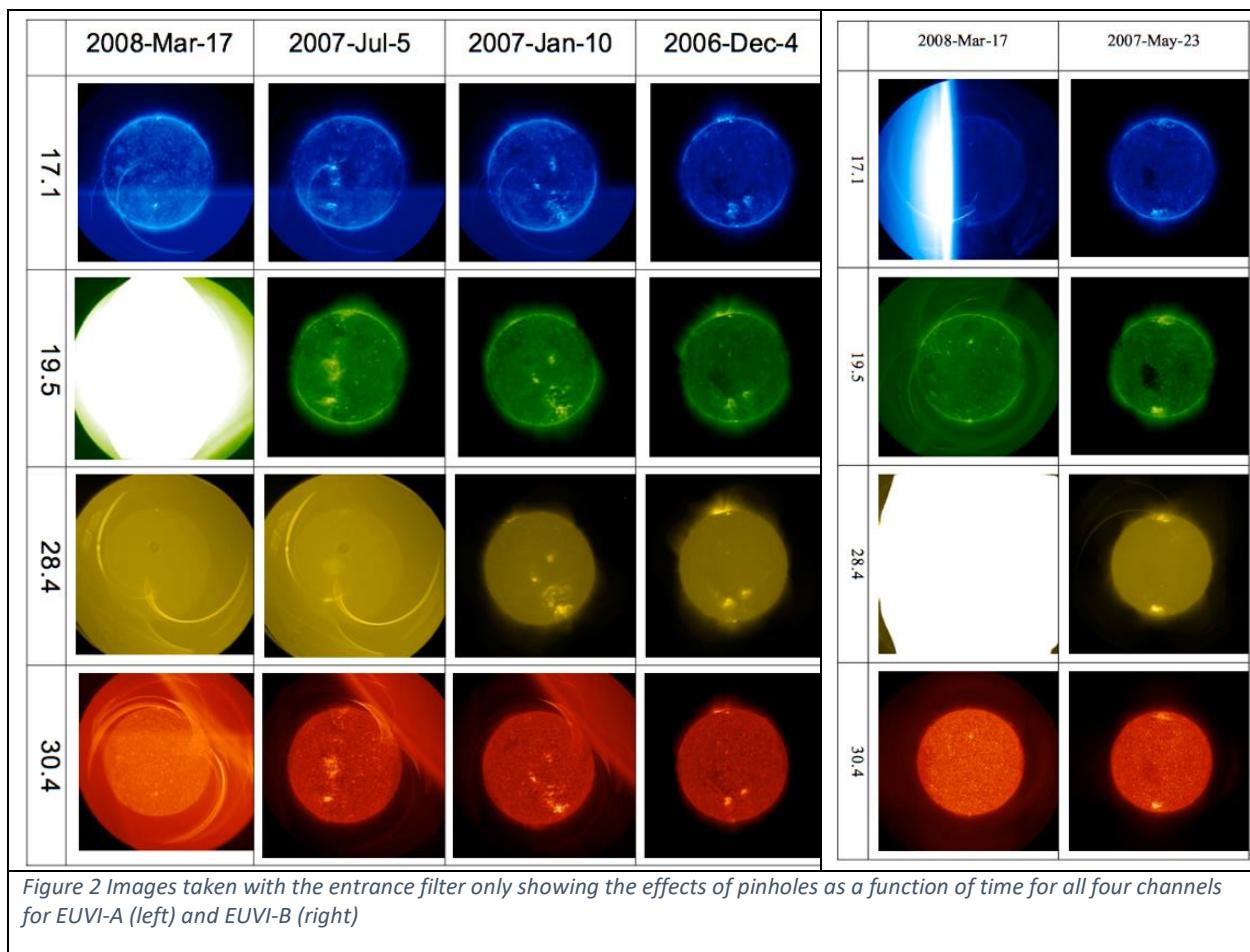
$$O = \frac{(I - Bias)}{t_{exp}} \frac{P_D}{N} V \tag{4}$$

Where V is a flat-field image to correct for vignetting and other effects (optional). Note that this equation does not take into account the detector conversion efficiency (i.e. no division by the QE). This is so that the output image, *O*, can be readily used for comparing with the expected response to plasmas of different properties for level-2 analysis, as discussed in A.3. Therefore, eq (4) returns 'detected' ph/s, not the incident photon flux on the detector.

2.3 Error Analysis and Corrections

Errors in the photometric calibrations can arise from increased stray light due to pinholes in the filters, improper filter selection in the filter wheel or reduction in the filter transmittance due to aging. All three factors are monitored via in-flight instrument-level calibrations at regular intervals as follows.

EUVI, uses two thin film filters to suppress out-of-band light; an entrance filter (Al+Poly on coarse grid for 171 & 195; Al on fine mesh for 284 & 304) and an analysis filter in a filter wheel close to the detector. Both filters are used in series during normal operations. All filters have developed pinholes over the years with EUVI-A 195 and EUVI-B 284 affected most. However, the pinholes have no impact on science observations as the analysis filters completely suppress out-of-band light. To monitor stray light and the condition of the entrance filters, images are taken occasionally with the analysis filters removed from the optical path (OPEN position). Last known trending analysis was performed in 2010 (Figure 2).
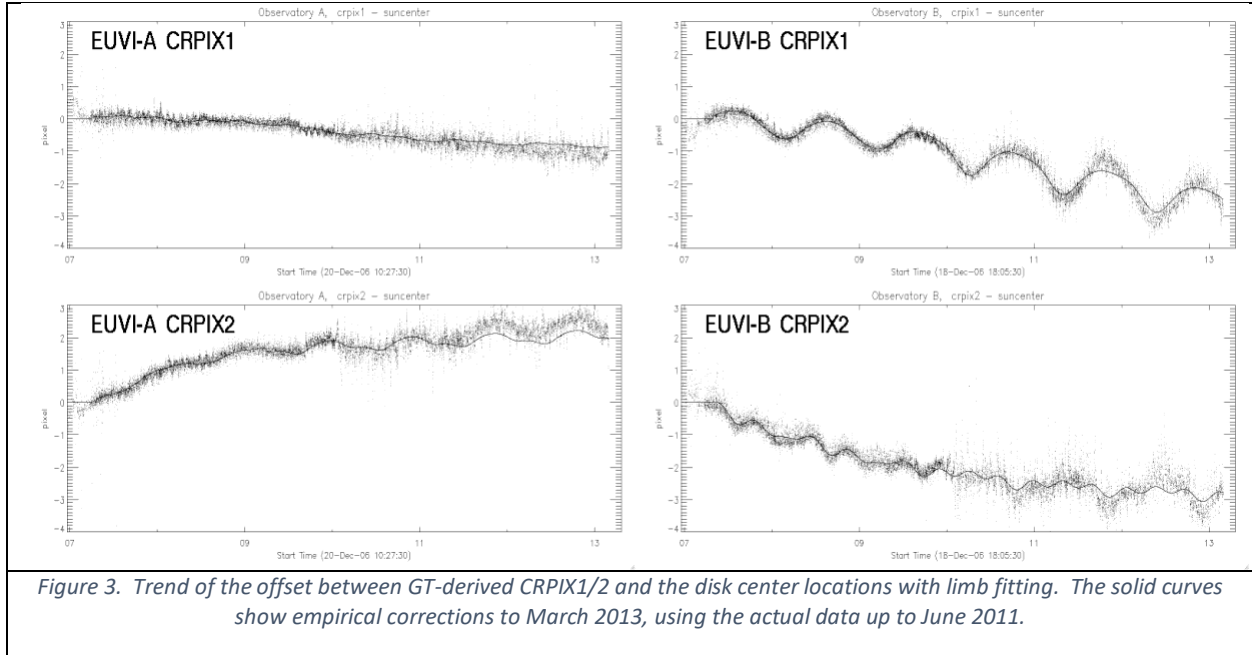

Figure 2 Images taken with the entrance filter only showing the effects of pinholes as a function of time for all four channels for EUVI-A (left) and EUVI-B (right)

EUVI_PREP (Eq (4)) has an option to carry out flat field correction by explicitly calling calibration images. These images are derived using the method of Chae (2004) from images acquired via spacecraft offpoints on April 16, 2008. At this point, only the flat field images for 171 and 304 nm channels are available in solarsoft. The 195 and 284 channel images will be provided by the next update of this document.

There are two versions, raw (_raw*) and processed (_grd*). The raw images contain the shadowing the mesh in the filter wheel filter and a faint residual solar image and they are noisy near the edge of field (due to low photon counts. The noise is further exaggerated by data compression. It is generally agreed that using such calibration images does more harm than good. The processed images are treated with fourier filtering to keep the mesh shadowing only. The effect is less that 4% of the peak signal (much less that the similar effect on the SOHO/EIT images). As it is generally unnecessary to flat field the EUVI images, this option is off by default. The processed calibration images should be used, if the removal of the mesh shadowing is important for a particular analysis.

Other corrections concern the pointing (knowledge and jitter).

For pointing correction, the CRPIX1 and CRPIX2 values in the header after secchi_prep are compared with the disk center locations obtained by limb fitting (see Figure 3). Errors in pointing correction, if exceeding two full-resolution pixels, are also revealed in running difference images after the images are registered using the header information. Running difference movies in half resolution (2x2 summation) at various times indicate that the errors in pointing correction (including the dejitter switch in euvi_prep described below) have been less than 2 in both CRPIX1 and CRPIX2 before and after the great conjunction.

EUVI_PREP first updates the pointing information in the header as performed by the routine EUVI_POINT. This is to make empirical corrections to the disk center location (in pixel coordinates) in the header as CRPIX1 and CRPIX2 which is initially derived using the output of the Guide Telescope (GT). The offset between the initial (CRPIX1, CRPIX2) and the disk center location as obtained by fitting the limb is shown in Figure 3. The variation of the GT axis location on the EUVI CCD depends on the GT front end temperature. Using the output of the EUVI Fine Pointing System (FPS), empirical corrections are made. The solid lines in Figure 3 show such corrections using the trend up to June 2011. They were good to ~0.5 pixels up to March 2013. Corrections reflecting the post-conjunction configurations were implemented in July 2015 for STEREO-A. EUVI_POINT is used in the pipeline processes, so CRPIX1 and CRPIX2 in the level0 header already reflects the empirical corrections described above, so calling it the second time in EUVI_PREP is to further update CRPIX1 and CRPIX2 in case spacecraft attitude files were missing in the pipeline.

Figure 3. Trend of the offset between GT-derived CRPIX1/2 and the disk center locations with limb fitting. The solid curves show empirical corrections to March 2013, using the actual data up to June 2011.

It was found, especially for data in the post-conjunction period, that there were considerable image motions even after correcting the header information using EUVI_POINT. These motions stood out in difference images. In order to reduce such image motions, a new switch "dejitter_on" was added in EUVI_PREP (but outside EUVI_POINT). This makes use of the output of the FPS and shifts the images accordingly.
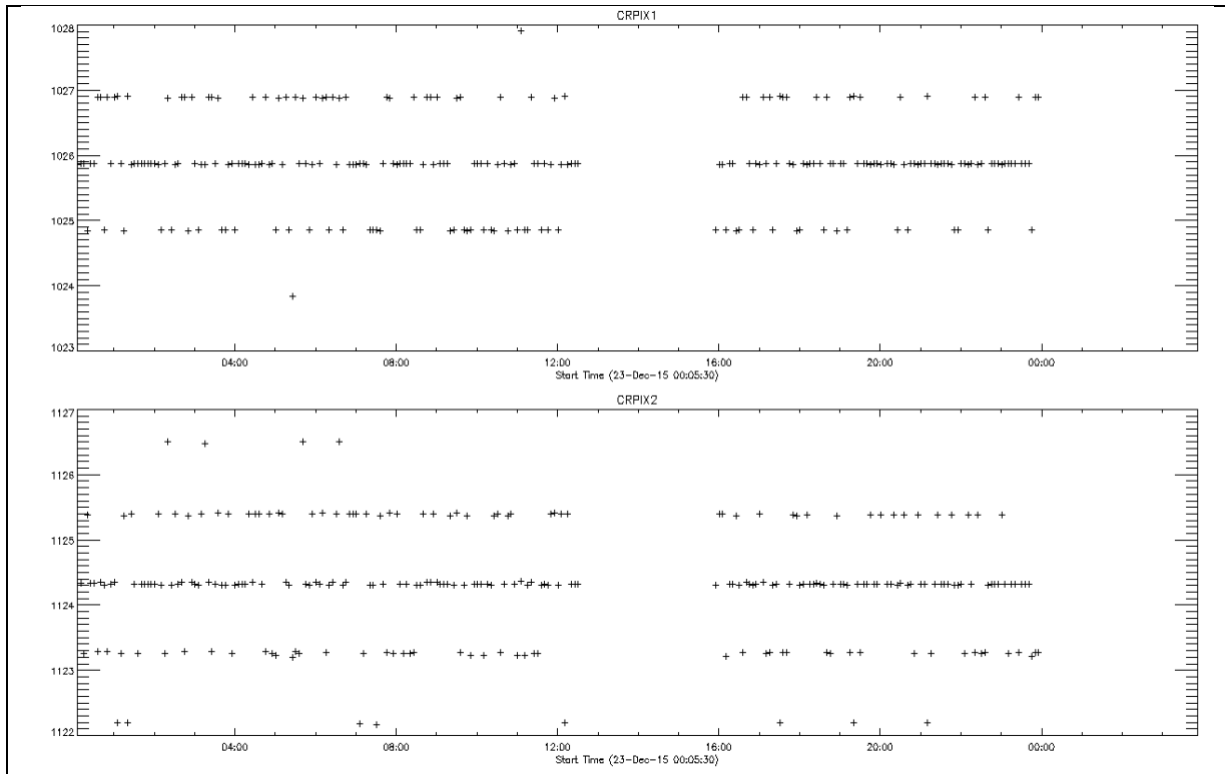
Figure 4. Calculated Sun center pixel locations for a sample date in December 2015

The EUVI fine pointing system sets the secondary mirror roughly to an integer pixel position at the beginning of each exposure. The rationale was as follows:

- The fine pointing system (FPS) has a limited range, so it was considered prudent to reset it for each exposure
- The reset is done in a fashion that any pointing jumps between images would be roughly integer values of a pixel. That way one could just shift the images without resorting to interpolation.

During the main part of the mission, the STEREO pointing was so good that jumps between images were quite rare. This changed when the S/C started operating without the gyros. Figure 4 shows the pixel location of Sun center as derived from the guide telescope for a sample date in December 2015, demonstrating that the pointing does indeed jump in increments of one pixel. This allows images to be aligned with their neighbors by applying a simple image shift. The amount of shift is determined from the parameters FPSOFFY and FPSOFFZ in the FITS headers, which show the offset of the EUVI fine pointing system in S/C coordinates and units of 2e-7 radians. Division by 38 gives the pixel offsets.
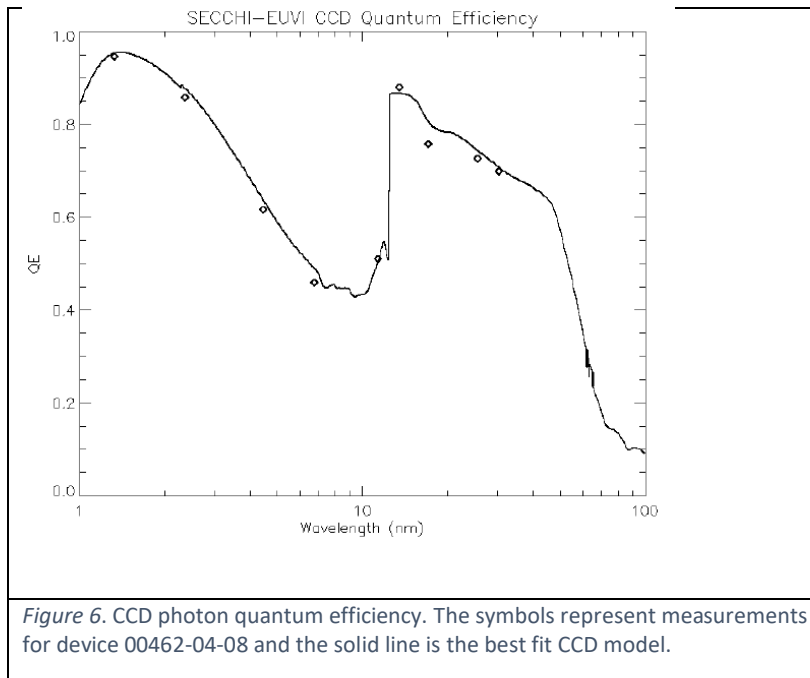
2.4 Calibration and Validation

2.4.1   Calibration

2.4.1.1 Ground Calibration

Figure 5 Calibration of the EUVI mirrors
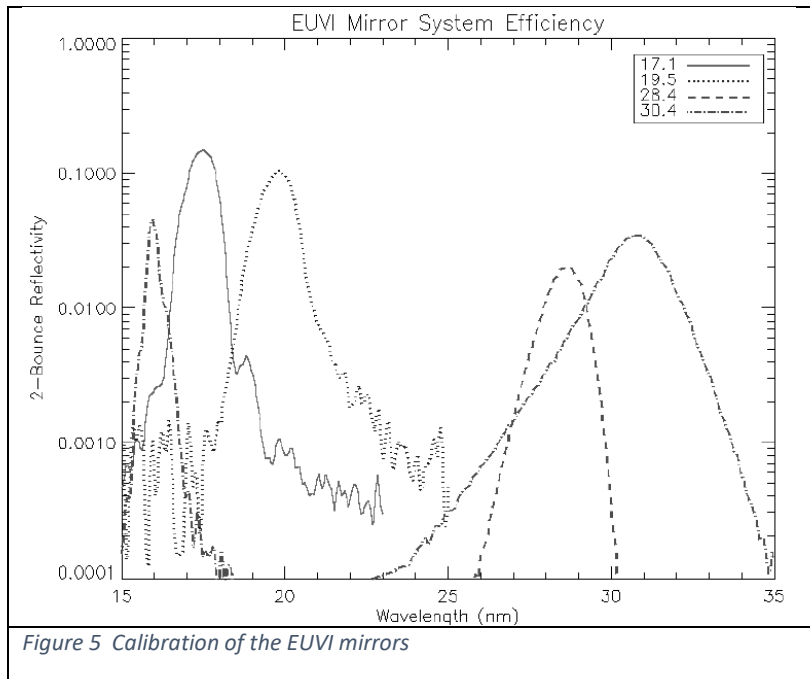
The pre-flight calibration of the EUVI instruments is described in Wuelser et al. (2004). It involves the mirror spectral reflectivity, the CCD performance and the filter transmission. The EUVI mirrors were calibrated as pairs at the synchrotron of the Institut d'Astrophysique Spatiale in Orsay. The results for the first flight mirror set are shown in Figure 5. The peak reflectivity is 39%, 35%, 15%, and 23%, respectively, for the 17.1nm, 19.5nm, 28.4nm and 30.4nm channels.

Figure 6. CCD photon quantum efficiency. The symbols represent measurements for device 00462-04-08 and the solid line is the best fit CCD model.

The CCDs were calibrated at the Brookhaven synchrotron and at the LMSAL XUV calibration facility Figure 6 shows the measured CCD quantum efficiency (symbols), and a CCD response model (Stern et al. 1994) fitted to the measurements (solid line).

The filter transmission was measured at LMSAL for the 171 channel only (0.5 for single, 0.25 for double width filters). The mirror reflectivity was measured at IAS, France. It was 0.11 for both mirrors. (primary/secondary).
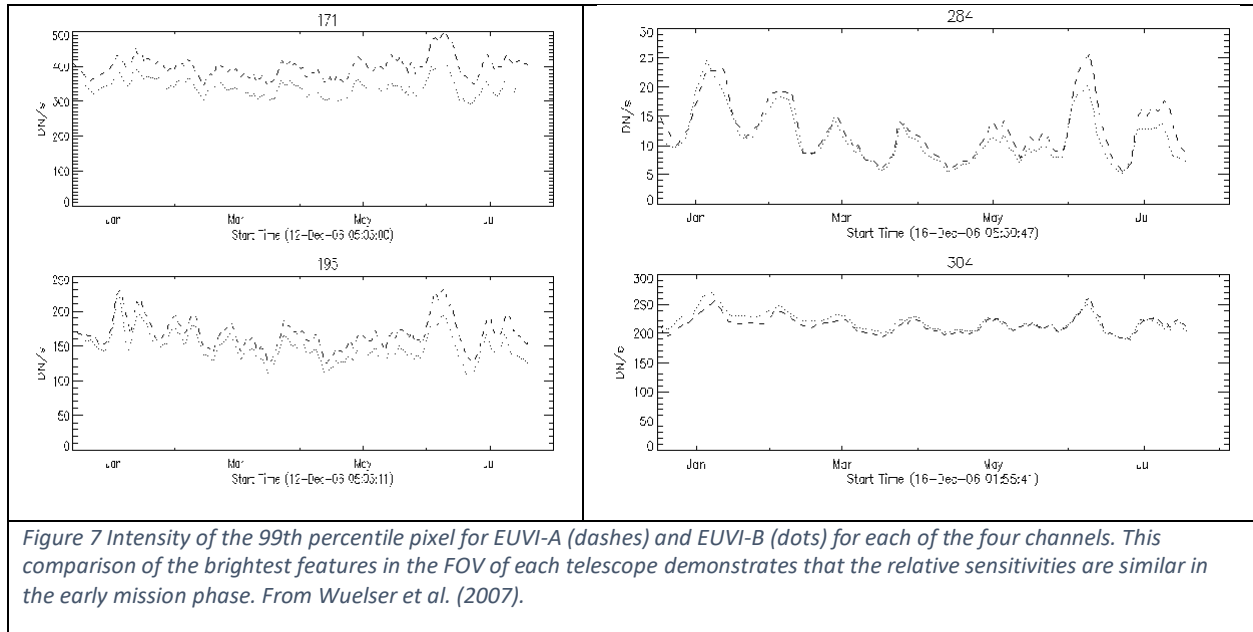
2.4.1.2 In flight Calibration

The in-flight calibrations performed so far is described in Wuelser et al (2007). These include EUVI-A and -B cross calibration and sensitivity analysis, determination of the PSF and trending of the straylight and throughput. EUVI-A and B intensities are within 10% of each other (Table 1).

Table 1 EUVI-B/EUVI-A Sensitivity Ratios (from Wuelser et al. 2007)

Channel (Å)	171	195	284	304
B/A signal ration	0.91 +/- 0.03	0.95 +/- 0.03	0.96 +/- 0.08	1.08 +/- 0.03

The trending of filter pinholes and stray light is discussed in A.2.3 and shows no impact on the science quality of the images. The same result was reached by the trend of the intensity in the two EUVIs during the early phase of the mission (when the two telescopes were close enough to image the same EUV solar activity). There was no significant sensitivity loss over the first 6 months of the mission (Figure 7).
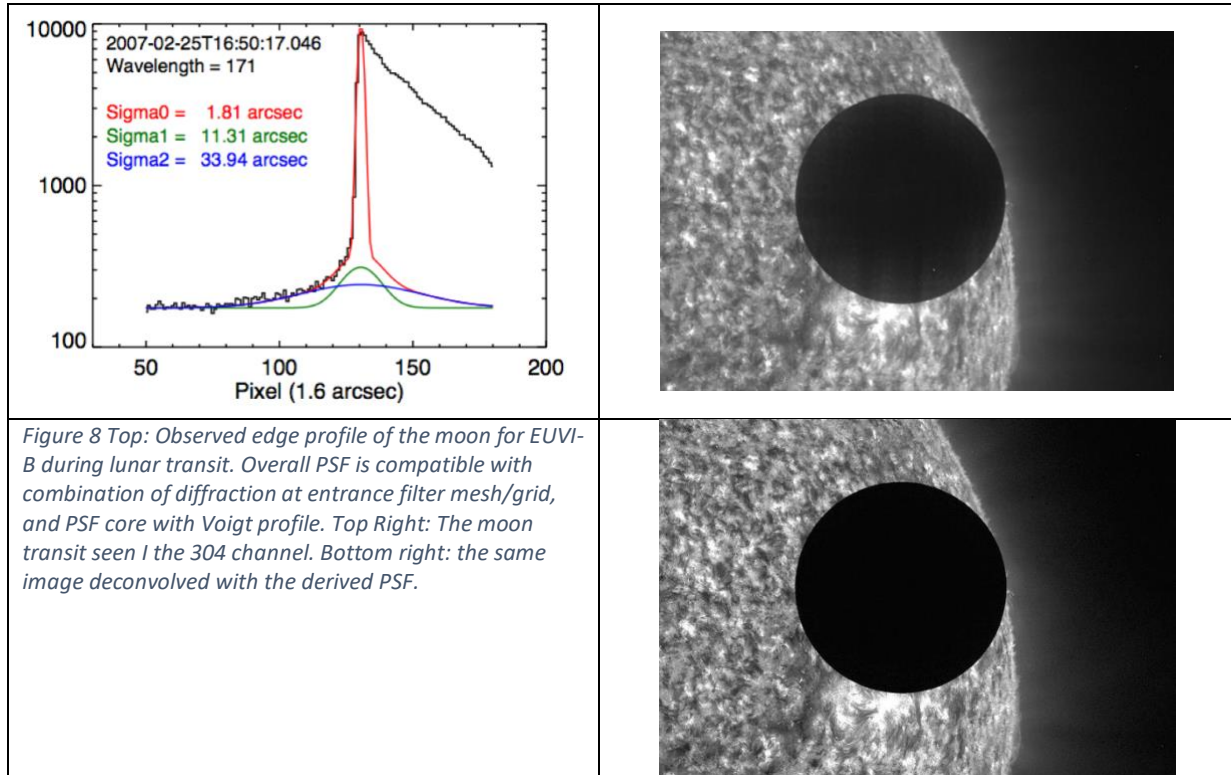

Figure 7 Intensity of the 99th percentile pixel for EUVI-A (dashes) and EUVI-B (dots) for each of the four channels. This comparison of the brightest features in the FOV of each telescope demonstrates that the relative sensitivities are similar in the early mission phase. From Wuelser et al. (2007).

2.4.2 Validation

Table 2 in-flight validation of the EUVI plate scale and roll orientation

Telescope	Plate Scale (arcs/pix)	Roll Angle(° CW from Solar North)
EUVI-A	1.5882 +/- 0.0005	- 0.12 +/- 0.03
EUVI-B	1.5904 +/- 0.0005	1.125 +/- 0.03

There has been no attempt yet to cross-calibrate EUVI with other EUV telescopes. A special observing programs was run during a calibration underflight of EUNIS-07 on November 6, 2007 but the data have not been analyzed yet. Cross-calibration with AIA (171 and 304, only) is also possible, which will allow to check the long-term stability of the calibration. These efforts will be completed before the next senior review and associated update of this document.

A moon transit over the solar disk early in the mission (February 25, 2007) provided an opportunity to derive the EUVI-B point spread function (PSF), roll calibration and validate the plate-scale. Simultaneous images from EUVI-A allowed the cross-calibration and validation of the plate-scale and roll for that

Figure 8 Top: Observed edge profile of the moon for EUVI-B during lunar transit. Overall PSF is compatible with combination of diffraction at entrance filter mesh/grid, and PSF core with Voigt profile. Top Right: The moon transit seen I the 304 channel. Bottom right: the same image deconvolved with the derived PSF.

telescope, as well. The measured plate-scale are almost identical to the nominal values validating the instrument focus. The results are given in Table 2. Figure 8 (left top) shows the profile of moon's edge during the transit and the fits to that edge that provide the PSF. The PSF core is described reasonably well by a Voigt profile. The results are implemented in the routine EUVI_PSF.PRO, which returns the best-estimate PSF for each wavelength and telescope and the PSF properties (diffraction pattern period, orientation, amplitude) based on the fits to observations. Figure 8 (right) demonstrates the effect of PSF deconvolution on a 304 channel image taken during the lunar transit.

2.5   References

[SECCHI_PREP] STEREO/SECCHI Level-0.5 to Level-1 Calibration CMAD, STEREO_SECCHI_Prep_CMAD_20211206.pdf, Version 1.1, 06 December 2021

Chae, J. Flat-Fielding of Solar Hα Observations Using Relatively Shifted Images. Solar Physics 221, 1–14 (2004). https://doi.org/10.1023/B:SOLA.0000033357.72303.89

Stern, R. A., Shing, L., Blouke, M. M., Quantum efficiency measurements and modeling of ion-implanted, laser-annealed charge coupled devices: x-ray, extreme-ultraviolet, ultraviolet, and optical data, Appl. Opt., 33, 2521, 1994

Wülser, J.-P., Lemen, J. R. & Nitta, N. The STEREO SECCHI/EUVI EUV coronal imager. in *Solar Physics and Space Weather Instrumentation II* vol. 6689 668905 (International Society for Optics and Photonics, 2007).

3. EUVI Temperature Response

3.1 Overview

Using the EUVI level-1 data as described in A.2, it is possible to relate the images to physical parameters. For example, we can estimate how much plasma of temperature T is contained in the image or in a given pixel in the form of emission measure (EM), $n_e^2 l$, where n_e is the electron density and l the line-of-sight length. The SolarSoft routine EUVI_FLUX.PRO gives the expected flux from (T, EM) , which is compared with the measurements in the level-1 images. Here we describe the two databases that EUVI_FLUX is based on.

3.1.1 Heritage

Starting from the Soft X-ray Telescope on Yohkoh in the 1990s, instruments operating in the soft X-ray or EUV wavelength ranges have adopted this approach of maintaining the effective area and temperature response databases for scientific analysis of the data.

3.1.2 Product Description

The expected output, in terms of photons or electrons, from plasma at a given temperature is calculated using the SolarSoft routine EUVI_FLUX. The routine uses the temperature response and effective area (Eq. (2)) of each EUVI channel to perform the calculation. The temperature response, *convolved with the effective area*, is stored in the so-called "sre" database. The instrument effective area is stored separately in the "sra" database. Both sra and sre files are SolarSoft-specific "geny" files that can be restored with the routine RESTGENX.PRO

3.2 Theoretical Description

The incident flux, F in equation (1) arises from a combination of emitting plasmas of density, *n,* and temperature, *T*, along the line of sight
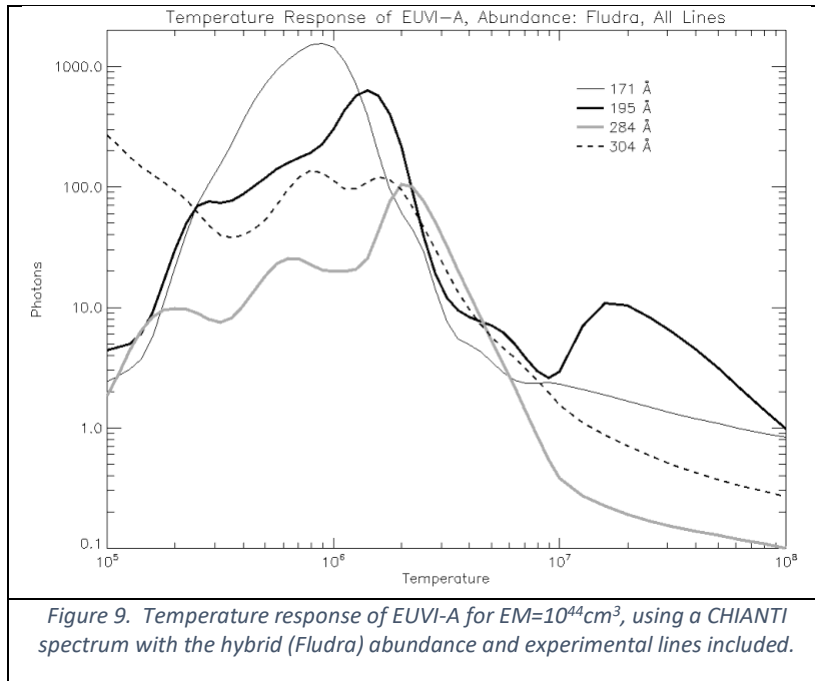
$$F(\lambda, n_e, T) = \int E(\lambda, n_e, T)\, DEM(T) dT \qquad (5)$$

Where $E(\lambda, n_e, T)$ is the theoretical emissivity of the plasma in photon cm^{-6} s^{-1} sr^{-1} Å^{-1} described by a differential emission measure, DEM(T) in cm^{-5}. *E* is computed for a wide range of temperature (0.3–100 MK) and different forms of photon spectra (APED (Smith et al. 2001) and CHIANTI (Dere et al. 1997) atomic databases; the latter with different abundances (coronal (Feldman) and hybrid (Fludra)) and whether to include experimental spectral lines). The expected response of the instrument (in DN/s/pix) in different channels and solar plasma properties can now be estimated from Eqs (1) and (5).

In the EUVI case, we follow a slightly different software procedure to be consistent with the overall *prep approach. As we explained in A.2.2, Eq (4) produces the level-1 O images calibrated in ph/s without accounting for QE for the following reason. From Eqs (1), (2), (4) and (5), we obtain

$$O = \frac{a_{pix}}{f^2} \int A_{eff}(\lambda)\, E(\lambda, T)\, DEM(T) dT \qquad (6)$$

Therefore, the correction for the detector QE (and the other losses in the optical path) is applied at this step. This operations is performed with the euvi_flux.pro procedure where different atomic models can be selected. The default set of keywords is CHIANTI, hybrid, experimental spectral lines (see Figure 9

Figure 9. Temperature response of EUVI-A for EM=10^{44}cm^3, using a CHIANTI spectrum with the hybrid (Fludra) abundance and experimental lines included.

3.3 Error Analysis and Corrections

The error analysis and corrections for the components (filters, mirrors) were discussed in A.2.3. The component-level estimate of the effective area (0.28 cm^2) was validated against an end-to-end (effective area) calibration using a monochromator for the 171 channel only (0.25 cm^2). Since the values are within 10% and the component calibrations is accurate to within 10-20%, there was no need for corrections.

3.4 Calibration and Validation
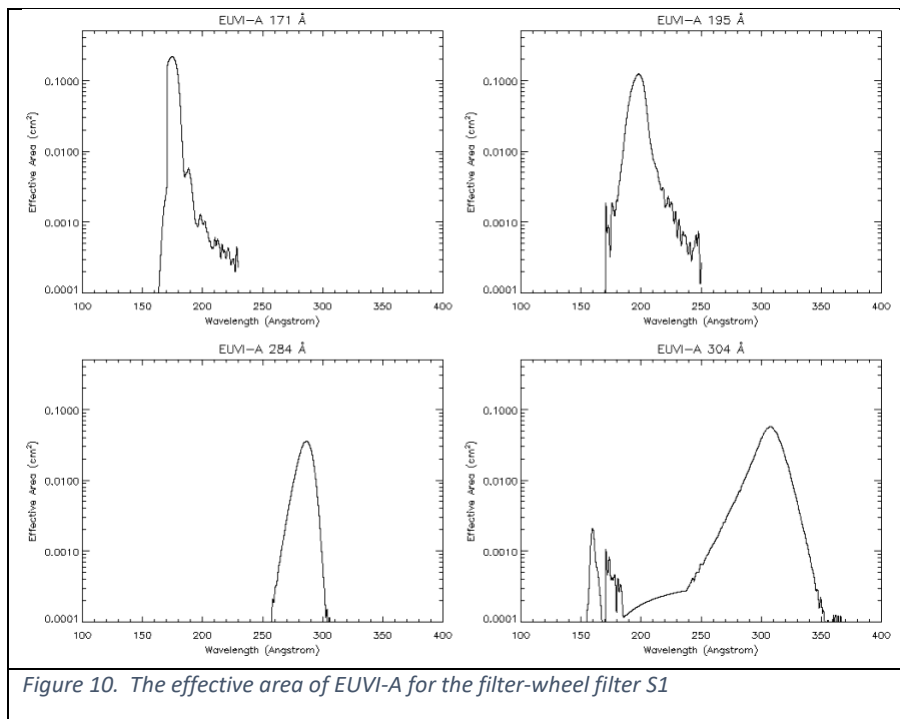
Figure 10. The effective area of EUVI-A for the filter-wheel filter S1

These are from prelaunch measurements, but in-orbit measurements were used to adjust the transmission of the filer-wheel filters of EUVI-B so that the overall response matched the observed ratios between EUVI-A and -B (adjustment between +4% and -19%). The effective area in the sra database is computed for a total of 16 combination of 4 wavelengths and 4 filter-wheel filters including OPEN. Figure 10 shows the effective areas of EUVI-A for the filter-wheel filter S1.

3.4.1   Validation

As we mentioned in A2.4.2, we have not performed yet a cross-calibration of the photometric response of EUVI to other telescopes. This effort will also validate the effective area values currently in use.

3.5   References

Dere, K. P., Landi, E., Mason, H. E., Monsignori Fossi, B. C., Young, P. R., CHIANTI - an atomic database for emission lines, Astron. Astrophys. Suppl, 125, 149, 1997

Smith, R. K., Brickhouse, N. S., Liedahl, D. A., Raymond, J. C., Collisional Plasma Models with APEC/APED: Emission-Line Diagnostics of Hydrogen-like and Helium-like Ions, Astrophys. J. Letters, 556, L91, 2001

4.   EUVI Wavelet

4.1   Overview

The EUVI images reveal a highly structured corona, both on the disk and off-limb. The structures evolve across multiple temporal and spatial scales, from seconds to days and from full Sun to the pixel resolution limit. These characteristics of solar EUV corona complicate the scientific analysis of the observations. The complications are compounded by instrumental background, such as scattered light from the optics and imprints from the filter grids and pinholes.

The scattered light is a particular concern for extended off-limb structures because the EUV intensity falls rapidly with height while the scattered light level remains relatively constant. The scattered light levels vary, generally, with heliocentric distance and solar activity. To enhance the visibility of the structures, mainly off-limb, with minimum photometric and other effects, we have developed a method to subtract the scattered light from the EUVI images, based on wavelet decomposition. This sections describes the method and results data products.

4.1.1   Heritage

The method was developed for the enhancement of the SOHO/EIT images and is discussed in Stenborg et al. (2008). It is described at some length in 4.2.

4.1.2   Product Description

The image processing algorithm is applied to every EUVI image, except for the beacon images, as soon as the Level 0.5 images become available at NRL. The images are downloaded to the APL server and processed via a set of IDL routines. The data are first calibrate, using SECCHI_PREP, and then processed through the wavelet decomposition algorithm, as discussed in the next section. The resulting images are stored in PNG and FITS format in channel/spacecraft-specific directories (e.g. 171_A) under YYYYMM/DD directories.

FITS files: The filename format (say, for 171A) is YYYYMMDD_HHMMSS_171eu_R.fts,gz, where R (L) stands for STEREO-A (B) image. The R/L convention was adopted for the use of these images with the stereoscopic software during the early phase of the mission. The FITS header is identical to the FITS header of the original EUVI image so it can be used seamlessly by the secchisoft software routines. The

data array is FLOAT type and the units are relative to the background model. In other words, the procedure retains the relative but not the absolute photometry.

PNG images: The filename format (say, for 171A) is YYYYMMDD_HHMMSS_171eu_R(L).png. The images are byte-scaled (0-255) arrays of the FITS data. They are used to build quick-look movies, either via scc_pngplay.pro (using '171_wa' or '171_wb' for the telescope) or via the online interface.

The FITS/PNG images are archived at the APL site and mirrored at the STEREO GSFC Science Center site. A third data product is a set of movies with two-wavelength combinations of the wavelet-processed movies for each spacecraft ('2-color' movies, see Figure 11). The combinations are 304-284 (min and max temperature responses), 304-195 (min and maximum emission measure) and 171-195 (complimentary fine-scale structures). Each movie in the three channel combinations covers a single month at one-hour cadence at 1024x1024 format (2x bin). The movies are available from the start of science operations (March 2007) to now at the wavelet-dedicated APL page.
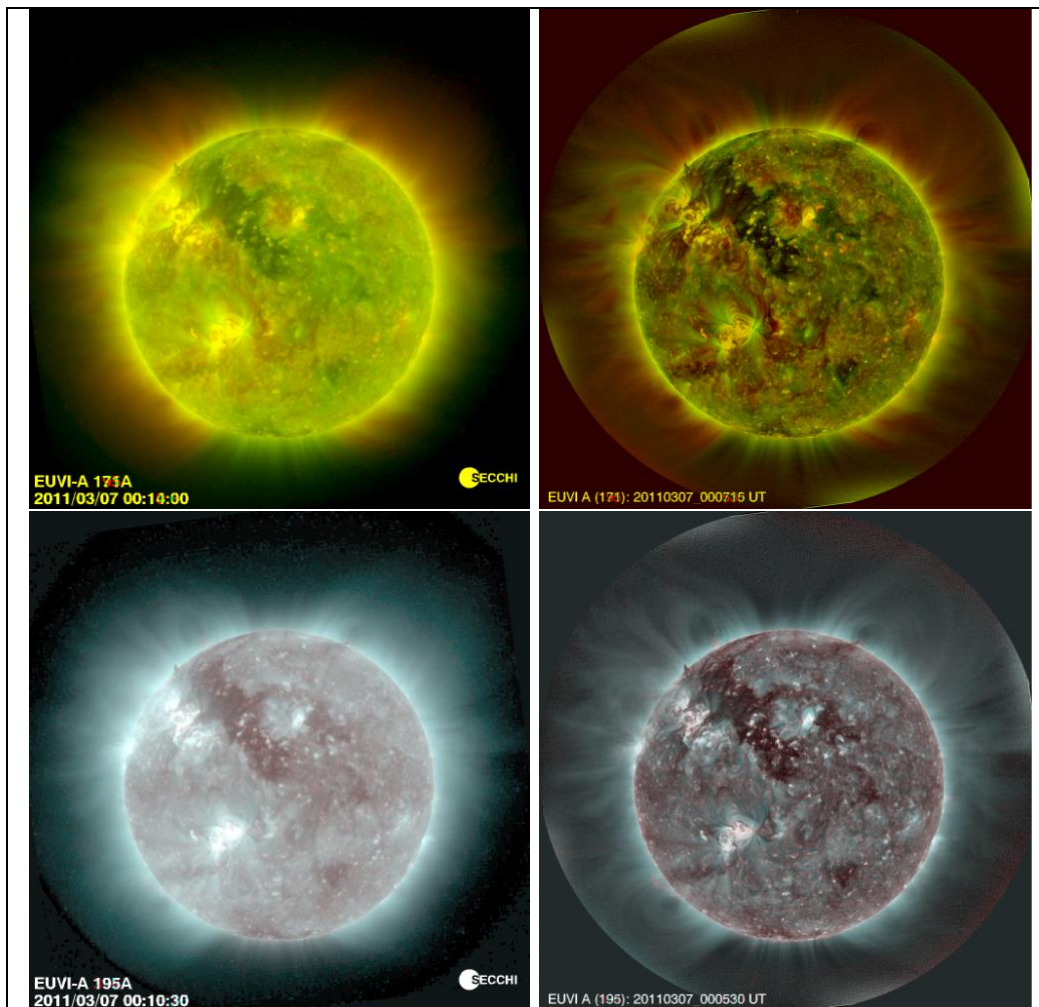

Figure 11 Example of STEREO EUVI-A blended (2-color) images. Top: 171A (yellow) / 195A (red). Bottom: 304A (red) / 195A (blue). Left: frames processed with the standard EUVI calibration routines. Right: frames processed further with the wavelets algorithm. Monthly movies are available online.

4.2　　Theoretical Description

The standard wavelet-processing approach involves the decomposition of an image into a set of spatial scales via the convolution of the image with kernels of varying size. Details can be found in many image processing textbooks. For this application, we are concerned only with stray light, which forms a broad and diffuse intensity background. The largest scales are captured by the first wavelet kernel and hence we only subtract this wavelet level from the image. Thus, we avoid influencing the finer spatial scales that may contain useful scientific information. The method proceeds as follows:

Let I_k denote a standard EUVI image at a given wavelength processed with the standard EUVI_PREP routine (i,.e., dark current subtraction, exposure time normalization, degrid, flat field, and degradation corrections). Then, for a one-level decomposition scheme, the reconstruction recipe to obtain the enhanced EIT images is (Stenborg et al., 2008):

$$I_k^{enhanced} = [\log(I_k > 0) - \beta \log(R > 0)] + \sum \alpha_j \, w_j$$

where w_j (j = 1, 2, ..., n) denotes the wavelet scales (i.e., the frequency components) obtained via the a` trous continuous wavelet transform (Holschneider & Tchamitchian, 1990; Shensa, 1992), and αj the weight given to the corresponding wavelet scale wj. Each individual image I_k is corrected by an appropriate model R to minimize the residual scattered light and effects of instrumental noise not properly addressed by the calibration routines. The model subtraction is weighted by a factor β ($\beta \leq 1$) determined by trial and error. The model R is derived for EIT from the minimum at each pixel over a solar rotation. However, the eccentricity of the STEREO orbit (which is larger than that of SOHO) prohibits the creation of the models in the same way as for the EIT images. For certain periods (in and around perihelion in particular), the change in size of the solar disc in the EUVI images is noticeable during a single month.

To circumvent this issue, we devised a procedure to obtain the model *R* directly from each EUVI image. The model is created using an iterative recursive smoothing procedure, which consists of recursively convolving I_k with an appropriate 2D kernel until the intensity gradient variation, along any direction in the image, is of the order of the solar disk size. Thus, the model is simply a conveniently smoothed version of the original image, where only the most extreme low frequency components remain. The number of iterations *n* varies with the plate scale of the EUVI mage, type of kernel, and kernel size. A reliable model for a typical 2048 x 2048 EUVI image can be obtained with n ~ 500 using a 5 x 5 gaussian kernel.

The main benefits of the technique is that it removes the diffuse background, thus enhancing the visibility of the off-limb structures and it does so without subtracting an image obtained at a different time, thus reducing confusion from the natural variability of the EUV emission.

4.3　　Error Analysis and Corrections

N/A

4.4　　Calibration and Validation

The wavelet-processed images are not photometrically accurate. They should be used for feature/edge identification and kinematics or similar-type measurements.

4.5　　References

Holschneider, M., & Tchamitchian, P., Les ondelettes en 1989, pp. 102-124, ed. P.G. Lemari, Springer (Berlin/Heidelberg, 1990).

Shensa, M.J., The discrete wavelet transform: wedding the a` trous and Mallat algorithms, IEEE Transactions on Signal Processing, 40, 2464-2482, 1992

Stenborg, G., Vourlidas, A., & Howard, R., A fresh view of the extreme- ultraviolet corona from the application of a new image-processing tech- nique, The Astrophysical Journal, 674, 1201-1206, 2008.